Features in the Spectrum of Cosmic-Ray Positrons from Pulsars

Ilias Cholis,[1] Tanvi Karwal,[1] and Marc Kamionkowski[1]

[1]*Department of Physics and Astronomy, The Johns Hopkins University, Baltimore, Maryland, 21218, USA*
(Dated: December 4, 2017)

Pulsars have been invoked to explain the origin of recently observed high-energy Galactic cosmic-ray positrons. Since the positron propagation distance decreases with energy, the number of pulsars that can contribute to the observed positrons decreases from $O(10^3)$ for positron energies $E \gtrsim 10$ GeV to only a few for $E \gtrsim 500$ GeV. Thus, if pulsars explain these positrons, the positron energy spectrum should become increasingly bumpy at higher energies. Here we present a power-spectrum analysis that can be applied to seek such spectral features in the energy spectrum for cosmic-ray positrons and for the energy spectrum of the combined electron/positron flux. We account for uncertainties in the pulsar distribution by generating hundreds of simulated spectra from pulsar distributions consistent with current observational constraints. Although the current *AMS-02* data do not exhibit evidence for spectral features, we find that such features would be detectable in $\simeq 10\%$ of our simulations, with 20 years of *AMS-02* data or three years of *DAMPE* measurements on the electron-plus-positron flux.

Cosmic-ray (CR) antimatter provides a probe of new phenomena at high energies. Most antimatter CRs are produced via inelastic collisions of regular high energy CR nuclei with the interstellar medium(ISM) gas. The resulting stable particles from these interactions are referred to as CR secondaries, and the observed fluxes are well described by models [1–8]. However, the CR positron flux, and energy spectrum of the positron fraction $e^+/(e^+ + e^-)$, are inconsistent with conventional models which predict lower fluxes than are observed above 10 GeV. Since energy losses due to synchrotron emission and inverse Compton scattering are much more important for $e^\pm$ than for nuclei, the discrepancy between model predictions and measurements of the high-energy positron flux is expected to be local: it may be associated with the propagation of CRs in the $\sim$kpc^3 volume around the Solar System [9] or with the characteristics of CR $e^\pm$ sources in the same volume. These sources could be local supernova remnants (SNRs) [10–16], local pulsars [17–25] or particle dark matter (DM) [23, 26–41].

A number of observations suggest that SNRs are the primary source of Galactic CR nuclei with energies up to $O(100)$ TeV. Yet, SNRs can explain the positron fraction only if the metallicities of environments of recent SNRs within $\simeq$kpc are different from those averaged within 10 kpc [14, 15, 42, 43]. DM explanations for the CR positron excess are constrained by cosmic-microwave-background data [44–49] and γ-rays [50–52], but parts of the parameter space are still available. Pulsars are a natural source of hard CR $e^\pm$ injection into the ISM. However, at the highest observed energies, $\gtrsim 500$ GeV, only a few very local sources, including Geminga, Monogem, and Vela, would dominate the CR flux. With recent observations from HAWC [53, 54] and Milagro [55] of $\gtrsim 10$ TeV γ-ray halos at $O(10)$pc around Geminga and Monogem, we now have strong indications that CR $e^\pm$ exit the surrounding pulsar wind nebulae (PWNe) [56], with additional implications for both pulsar searches [57] and the TeV emission observed by HESS [58] towards the Galactic center [59].

Pulsars are born in the Milky Way at a rate of $\simeq 1$ per century [60–64]. This implies only one new pulsar every 10^3 years born within the 4-kpc distance that $\gtrsim 10$-GeV positrons can travel. Moreover, since the energy-loss timescale is ~ 10 Myr for $E \gtrsim$ GeV positrons, no more than $\sim 10^4$ pulsars can contribute positrons with energies above a few GeV. Above 100 GeV the equivalent distance drops to 2 kpc and the maximum age to 2 Myr, and above 500 GeV to 1 kpc and 400 kyr. Thus, as we go to higher energies, the number of candidate pulsar sources decreases. Since energy losses and diffusion provide a rough maximum $e^\pm$ energy $E_{\max} \sim 100 \, \text{GeV} (R/2 \, \text{kpc})^{-2}$ from a pulsar at a distance R, the discreteness of the source population shows up as spectral features in the CR spectra [20, 21]. This is illustrated schematically in Fig. 1. These, moreover, cannot be mimicked by dark-matter (even if there are multiple DM particles) [39, 65].

The red-curve in Fig. 1 shows an example of the type of features in the energy spectrum that may be induced by discreteness of the source population. Shown is the positron energy spectrum for a simulation of pulsars born within 4 kpc from the Sun at a rate of 1 kyr^{-1} (red line). Roughly speaking, the amplitude of the wiggles increases as the number of sources contributing to the local positrons decreases. We also show for comparison the prediction from an example DM annihilation model (green line) from Ref. [23] typical of [31, 32, 40, 66]. Both the DM and the pulsar models give good fits to the *AMS-02* measurement. Even after 20 years of data taking, given the combined statistical and systematic errors [67], *AMS-02* will not distinguish the DM model from the smoothed version of the red curve. The red curve may, however, be distinguished through the presence of the wiggles.

In this *Letter*, we suggest a power-spectrum technique to search for wiggles in the positron energy spectrum induced by discreteness of the source population. To illustrate, we perform 900 simulations of the Milky Way pulsar population accounting for the astrophysical uncertainties in this population. We then evaluate the prospects to detect, with this power-spectrum analysis,
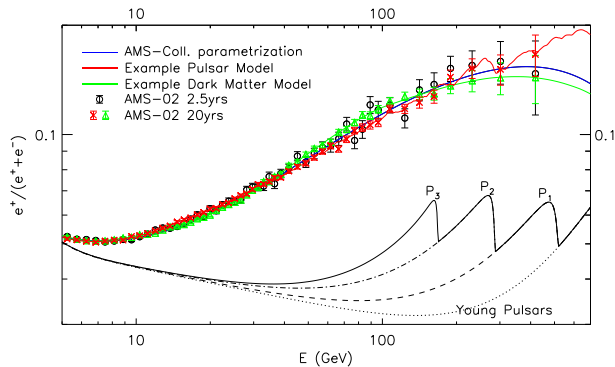
FIG. 1. The *AMS-02* positron fraction measurement (black data) [67] and two examples of models that fit it well. The red line is from the contribution of many Milky Way pulsars, while the green line is from a sample DM model (see text for details). The DM spectrum is genuinely smooth, while the pulsar spectrum shows evidence of the contribution from individual sources at high energies. The curves labeled P_1, P_2 and P_3, illustrate schematically the contribution from individual pulsars, at distances of 0.66, 0.97 and 1.7 kpc and ages of 240, 430 and 740 kyrs, respectively. The three pulsars contributions are enhanced for illustrative purposes. The dotted "Young Pulsars" line show the contribution from pulsars with ages less than 150 kyrs. We show what a measurement of each model would be after 20 years with *AMS-02*. We would not be able to separate them through a fit to the spectrum. We also show the AMS-Collaboration parametrization [67].

pulsar-induced wiggles. While current data are unlikely to have sufficient sensitivity, we find that the prospects to detect the wiggles with forthcoming data are good enough to warrant a careful analysis.

Data: We use published *AMS-02* data [67] that stem from 2.5 years of measurements from 5 GeV and up to 500 GeV. We also simulate for 20 yr assuming the same energy bins and percentage systematic errors. We also project three years of spectral measurements of the combined $e^\pm$ flux, up to 1 TeV, by *DAMPE*. We work with binned data, there may be benefits, in a realistic analysis, to working with the raw data, especially if the bin widths exceed the instrumental resolution.

Pulsar-population uncertainties: The pulsars contribution to the local CR spectra, has several uncertainties. There are uncertainties on the neutron-star distribution in the Milky Way [62, 63, 68] and their birth rate [60–64]. For the spatial distribution we follow Ref. [63], which relied on data from Ref. [69], and take a birth rate of 1/century. For further details see Appendix A. There are also uncertainties regarding the neutron stars' initial spin-down power $\dot{E}_0$, braking index κ, and spin-down timescale τ_0, that all relate to the time t-dependence of the spin-down power,

$$\dot{E}(t) = \dot{E}_0 \left(1 + \frac{t}{\tau_0}\right)^{-\frac{\kappa+1}{\kappa-1}}. \tag{1}$$

We assume that $\dot{E}_0$ follows a distribution $f(\dot{E}_0)$, which

we vary, in addition to varying κ and τ_0, ensuring that no pulsar has a spin-down power higher than the recorded ones [70, 71]. For further details see Appendix B.

Only a small fraction η, of the spin-down power can go to injected CR $e^\pm$ into the ISM. The CR $e^\pm$ before entering the ISM may be accelerated by the surrounding PWN and for younger pulsars the SNR shock front further out; this leads to significant uncertainties in the CR injection spectra. For each pulsar we assume a unique η and energy spectrum $\frac{dN}{dE}_{e^\pm} \propto E^{-n} Exp\{-E/E_{\rm cut}\}$, where η and n are described by equivalent distributions (i.e. no two pulsars in our simulations have identical η or n). We test different variations on these distributions (details are provided in Appendix C). Finally as CR $e^\pm$ enter the ISM, they must propagate to the Earth where they are observed. There are uncertainties regarding the CR diffusion, energy-losses and the impact of the time-evolving Heliosphere. We have different assumptions to model the propagation through the ISM, using [20, 72], while we account for the uncertainties of the propagation inside the Heliosphere (i.e. Solar Modulation [73]) by marginalizing over them following [72] and [42]. For the time-evolution of the heliospheric magnetic field we use information from Ref. [74, 75] (relevant details in Appendix D).

Given a spatial distribution and pulsar birth rate, a distribution $f(\dot{E}_0)$, choices for κ and τ_0, distributions on the fraction of spin-down power that goes into ISM CR $e^\pm$ $g(\eta)$, distribution $h(n)$ on the injection index n, and choice of ISM propagation models, we generate a population of Milky Way pulsars that are within 4 kpc. To understand the impact of these uncertainties on the prospects to detect fluctuations in the positron energy spectrum, we produce 900 astrophysical realizations. Each one has a unique combination of the above ingredients while still consistent with pulsar population studies [62] and data on CR propagation in the ISM and the Heliosphere [76].

Technique: We fit the pulsar contribution to the *AMS-02* positron-fraction[1] by allowing for an additional normalization on the $e^\pm$ pulsar flux and by marginalizing over the uncertainties of primary and secondary CRs and Solar Modulation. That alone constrains a significant fraction of the pulsar astrophysical realizations, if they are to explain the positron fraction. We leave that discussion for subsequent work [77]. Of the 900 pulsar astrophysical realizations, only 172 fit the positron fraction within 3σ from a prediction of 1 per degree of freedom.

———————

[1] In principle, the analysis may be optimized by working with the positron flux itself, rather than the positron fraction, as the fluctuation amplitude is suppressed given that fluctuations in the electron spectrum will be similar. Still, (a) most electrons in the relevant energy range are not from pulsars, and so the suppression is small; (b) most publicly available current results are provided in terms of the positron fraction; and (c) some systematic effects that might introduce artificial fluctuations may be canceled out by working with the positron fraction.

For the remainder of this analysis, we use those pulsar astrophysical realizations, one of which is shown in Fig. 1. Our results are not sensitive to the exact threshold that we place on the χ^2 of the fit.

For each of the remaining 172 pulsar astrophysical realizations, we generate 10 observational realizations (i.e. add noise following the binning and errors of Ref. [67]); this can generate artificial fluctuations that mask the wiggles we seek. We then subtract from each observational realization the smoothed spectrum and evaluate the power-spectral density (PSD) of the residual spectrum. Since we do not know the true underlying astrophysical spectrum, we calculate for each realization the smoothed spectrum by convolving with a gaussian whose width increases with energy. This removes power in large scales in energy (low modes in the power spectrum) including contributions from instrument systematics as misestimates of the instrument efficiency or CR contamination.[2]

To evaluate the PSD on the residual positron spectrum, we take the "time" parameter to be $ln(E/\text{GeV})$ which we assume to be measured in equal intervals. This is to a very good approximation true in the energy range 5–150 GeV, with higher energies having energy bins at larger separations. In our calculations we assume a logarithmic energy binning of $ln(E_i/\text{GeV}) \equiv x_i = x_0 + a \cdot i$, with $x_0 = 1.6571$ (5.24 GeV) and $a = 0.063$. When comparing to current data, we go up to $i = 59$ (215 GeV) while in our 20-year forecast we go up to $i = 65$ (315 GeV). We calculate the PSDs for each of the 172×10 observational realizations. Given the noise, there is scatter on the PSDs of the 10 observational realizations coming from the same underlying astrophysical realization.

To model the effect of observational scatter on the PSD, we use the *AMS-02* smooth parametrization that fits well the data after 2.5 years and then produce 200 observational realizations of it. We then calculate the 200 PSDs on the residual. Those 200 observational realizations of the *AMS-02* smooth parametrization provide the scatter on the PSD due to noise. For every one of the 60 (66) modes for the current (20 yr) data, we rank the 200 coefficients.[3] We use the 68% ranges to derive the 1σ error-bars per mode. We then determine a χ^2 fit on each of the PSDs. Among the 200 observational realizations of the *AMS-02* smooth parametrization there is a median in terms of its χ^2 and 68%, 95% and 99% ranges. We use these ranges to *compare* the PSDs from physical models (pulsars or DM) and the PSD from noise. These ranges provide a measure of the scatter due to noise and whether pulsars can give a PSD signal above the noise.

Results: In the left panel of Fig. 2 we show the PSD of the measured *AMS-02* positron fraction from the *AMS-02* smooth parametrization (black line). The PSD of

---

[2] Systematic artifacts in a small number of energy bins could still induce smaller-scale fluctuations that we seek.

[3] We do not expect any correlations between modes.

Experiment	E-range (GeV)	# freq. modes	% excl. fr. (95%)	% excl. fr. (99%)
AMS-02 (2.5 yr)	5.2-215	±30	12.5	3.5
AMS-02 (20 yr)	5.2-315	±33	10	6
DAMPE (3 yr)	25-640	±19	12	7

TABLE I. The potential to observe power from small-scale features to the residual positron fraction (for *AMS-02*) or $e^+ + e^-$ flux (for *DAMPE*). We give the relevant energy range to be used, the # of modes ($\pm 1/2$ the number of logarithmically spaced E-bins). " % excl. fr." gives the % of realizations that fall outside the 95% and 99% noise ranges.

the noise realization with the median fit is given by the blue line. We also show the PSDs for the pulsar astrophysical realization and the DM model of Fig. 1 adding noise (red and green lines, respectively). As seen there, pulsars produce small-scale (small in $ln(E/\text{GeV})$) variations that lead to extra power in the PSD at high modes (large $f = 1/ln(E/\text{GeV})$). The exact DM phenomenology (i.e mass annihilation/decay channel) can only affect the lower modes. DM models with one very evident and sharp spectral feature that could add some power are already excluded in Ref. [78, 79]. The difference between the red and the green PSDs on the residual positron fraction is what we are interested in. With 20 years of data the situation improves, as shown in the right panel of Fig. 2, for a 10% chance to see these fluctuations if pulsars are responsible for high-energy CR positrons.

In Fig. 3 we show for all 172 pulsar astrophysical realizations and for each of the 10 observational realizations the PSD χ^2-distribution (red diamonds along y-axis). Each pulsar astrophysical realization is in a different position on the x-axis; ranked starting with the model that fits best the positron fraction spectrum. We also show 10 observational realizations of the sample DM model (green triangles). Our calculation of the fit of the observed *AMS-02* PSD on the residual positron fraction is given by the black line. All triangles, diamonds, and the black line are to be compared to the three blue bands that represent the 68%, 95% and 99% ranges of the noise. We find that with current data 3.5% (12.5%) of the 172×10 observation realizations lie outside the 99% (95%) band (left panel of Figure 3). This information is also given in Table I. Since we have ranked our astrophysical realization models on the x-axis by their fit to the positron fraction, Fig. 3 also shows that there is no clear correlation between models that provide a poor fit to the smoothed energy spectrum and models that provide a poor fit to the power-spectrum. Also since the data PSD sits well within the 68% band of the noise, there is no indication yet that there is a deviation from a smooth spectrum; however, this null result cannot yet distinguish between different scenarios.

After 20 years of observations, and using information on the positron spectrum up to 315 GeV, the situation becomes more promising. Then, about 6% (10%) of the observational realizations sit within the 99% (95%) noise bands, as shown in the right panel of Fig. 3 and in Table I.
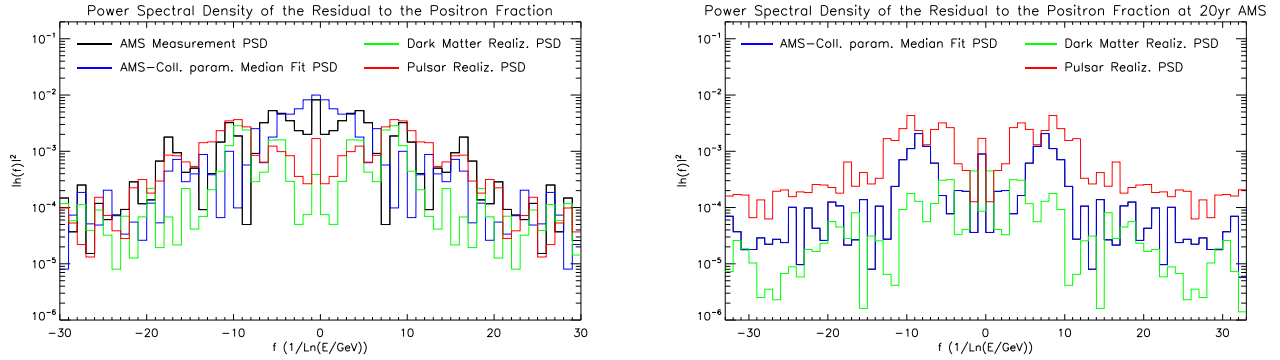
FIG. 2. The PSD of the residual to the positron fraction from *AMS-02*. *Left*: current state with the black line giving the measurement, the blue line the noise realization with median fit and the red and green lines a pulsars and a DM realization. Since pulsars have spectral features (shown in Fig. 1), there is more power at the high modes of the PSD compared to the smooth DM realization. *Right*: Same after 20 yr of *AMS-02* observations, for a $\sim$10% chance that a pulsar signal in the PSD can be detected.
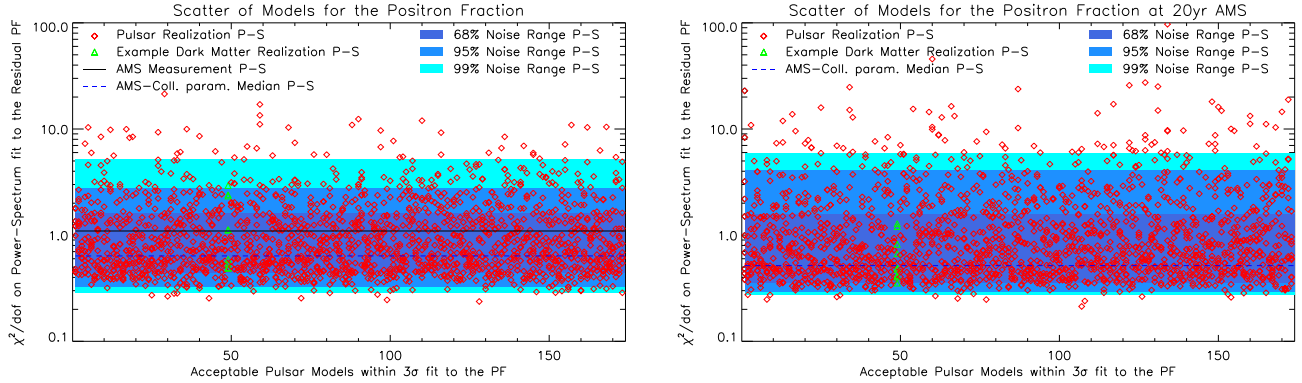

FIG. 3. The scatter of 10 observational realizations in the PSD χ^2/dof for each of the 172 pulsar astrophysical realizations (red diamonds) and the DM example (green triangles). The blue bands include the noise ranges for the PSD χ^2. *Left*: Current, with the black line giving the PSD of the measurement, showing no clear evidence for features. *Right*: After 20 years of data, $\sim 10\%$ of the pulsar realizations will provide detectable fluctuations.

DAMPE [80, 81] and *CALET* [82] are now measuring the total CR $e^+ + e^-$ flux up to several TeV. We forecast the prospects to probe a PSD signal from pulsars to higher energies where fewer pulsars contribute to the signal. Using the expected flux measurement between 25 and 640 GeV we find that 38 logarithmically equally spaced energy bins provides us with a good sensitivity to the presence of features.[4] Of the 172 pulsars realizations, 53 include at least one pulsar that has similar power, age and distance as Geminga (PSR B0633+17) and one with similar properties for Monogem (PSR B0656+14). We use that subset, since these pulsars are relevant for that range of energies but not for the energy ranges used for the *AMS-02* data. Our findings are given in Table I suggesting that indeed going to higher energies is necessary.

Discussion and Conclusions: In this *Letter*, we have proposed a power-spectrum analysis to identify wiggles in the positron energy spectrum that may arise

from discreteness in the pulsar source population, in the event that pulsars are responsible for high-energy CR positrons. Our basic conclusions are that although such wiggles are likely too small to be detectable with current data, the prospects to see such wiggles with forthcoming data warrant the effort such an analysis would entail.

Our estimates of the detectability of the signal rely on a variety of uncertain ingredients in the modeling of the pulsar-population. To obtain some indication of these uncertainties, we constructed 900 simulated pulsar-population realizations each obtained with different assumptions about the neutron-star distribution, spin-down power characteristics and time-evolution, the injected CR $e^{\pm}$ spectra, and propagation through the ISM and the heliosphere, but requiring consistency with all observational constraints in each simulation used in the analysis. Thus, while our forecast of a $\sim$10% chance to detect these wiggles is uncertain, it is, we believe, based on realistic models. The takeaway message is therefore that the possibility to see something in a PSD analysis is significant enough to warrant a search. It is not, however,

---

[4] Any further optimizations should be left to the collaborations.

certain enough to ascribe any strong conclusions to a null result. With better understanding of the astrophysics in the next decade, the forecast may become more, or less optimistic, but almost certainly more robust. This analysis can be repeated for SNR sources.

The predictions of wiggles are statistical only. We ascribe significance to the presence of wiggles, but we do not make predictions about specific features at specific energies. We also do not ascribe the signal to any specific pulsar (e.g., Geminga or Monogem), although our models are required to have pulsar-populations consistent with the existence of these pulsars. Also, we emphasize that we simply estimate the sensitivity of current measurements to a power-spectrum-based wiggle search.

We do hope, however, that this work motivates collaborations like *AMS-02* and at higher energies *DAMPE* and *CALET* to perform their own PSD analysis with their data.

[1] I. V. Moskalenko, A. W. Strong, J. F. Ormes, and M. S. Potgieter, Astrophys. J. **565**, 280 (2002), astro-ph/0106567.

[2] M. Kachelriess, I. V. Moskalenko, and S. S. Ostapchenko, Astrophys. J. **803**, 54 (2015), 1502.04158.

[3] http://galprop.stanford.edu/.

[4] A. W. Strong (2015), 1507.05020.

[5] C. Evoli, D. Gaggero, D. Grasso, and L. Maccione, JCAP **0810**, 018 (2008), 0807.4730.

[6] http://dragon.hepforge.org.

[7] C. Evoli, I. Cholis, D. Grasso, L. Maccione, and P. Ullio, Phys. Rev. **D85**, 123511 (2012), 1108.0664.

[8] M. Pato, D. Hooper, and M. Simet, JCAP **1006**, 022 (2010), 1002.3341.

[9] G. Di Bernardo, C. Evoli, D. Gaggero, D. Grasso, L. Maccione, et al., Astropart.Phys. **34**, 528 (2011), 1010.0174.

[10] P. Blasi, Phys. Rev. Lett. **103**, 051104 (2009), 0903.2794.

[11] P. Mertsch and S. Sarkar, Phys. Rev. Lett. **103**, 081104 (2009), 0905.3152.

[12] M. Ahlers, P. Mertsch, and S. Sarkar, Phys. Rev. **D80**, 123017 (2009), 0909.4060.

[13] P. Blasi and P. D. Serpico, Phys.Rev.Lett. **103**, 081103 (2009), 0904.0871.

[14] I. Cholis and D. Hooper, Phys. Rev. **D89**, 043013 (2014), 1312.2952.

[15] P. Mertsch and S. Sarkar, Phys. Rev. **D90**, 061301 (2014), 1402.0855.

[16] M. Di Mauro, F. Donato, N. Fornengo, R. Lineros, and A. Vittino, JCAP **1404**, 006 (2014), 1402.0321.

[17] D. Hooper, P. Blasi, and P. D. Serpico, JCAP **0901**, 025 (2009), 0810.1527.

[18] H. Yuksel, M. D. Kistler, and T. Stanev, Phys. Rev. Lett. **103**, 051101 (2009), 0810.2784.

[19] S. Profumo, Central Eur. J. Phys. **10**, 1 (2011), 0812.4457.

[20] D. Malyshev, I. Cholis, and J. Gelfand, Phys. Rev. **D80**, 063005 (2009), 0903.1310.

[21] D. Grasso et al. (Fermi-LAT), Astropart. Phys. **32**, 140 (2009), 0905.0636.

[22] T. Linden and S. Profumo, Astrophys.J. **772**, 18 (2013), 1304.1791.

[23] I. Cholis and D. Hooper, Phys. Rev. **D88**, 023013 (2013), 1304.1840.

[24] Q. Yuan, X.-J. Bi, G.-M. Chen, Y.-Q. Guo, S.-J. Lin, and X. Zhang, Astropart. Phys. **60**, 1 (2015), 1304.1482.

[25] P.-F. Yin, Z.-H. Yu, Q. Yuan, and X.-J. Bi, Phys. Rev. **D88**, 023001 (2013), 1304.4128.

[26] L. Bergstrom, T. Bringmann, and J. Edsjo, Phys. Rev. **D78**, 103520 (2008), 0808.3725.

[27] M. Cirelli and A. Strumia, PoS **IDM2008**, 089 (2008), 0808.3867.

[28] I. Cholis, L. Goodenough, D. Hooper, M. Simet, and N. Weiner, Phys. Rev. **D80**, 123511 (2009), 0809.1683.

[29] M. Cirelli, M. Kadastik, M. Raidal, and A. Strumia, Nucl. Phys. **B813**, 1 (2009), [Addendum: Nucl. Phys.B873,530(2013)], 0809.2409.

[30] A. E. Nelson and C. Spitzer, JHEP **10**, 066 (2010), 0810.5167.

[31] N. Arkani-Hamed, D. P. Finkbeiner, T. R. Slatyer, and N. Weiner, Phys. Rev. **D79**, 015014 (2009), 0810.0713.

[32] I. Cholis, D. P. Finkbeiner, L. Goodenough, and N. Weiner, JCAP **0912**, 007 (2009), 0810.5344.

[33] I. Cholis, G. Dobler, D. P. Finkbeiner, L. Goodenough, and N. Weiner, Phys. Rev. **D80**, 123518 (2009), 0811.3641.

[34] R. Harnik and G. D. Kribs, Phys. Rev. **D79**, 095007 (2009), 0810.5557.

[35] P. J. Fox and E. Poppitz, Phys. Rev. **D79**, 083528 (2009), 0811.0399.

[36] M. Pospelov and A. Ritz, Phys. Lett. **B671**, 391 (2009), 0810.1502.

[37] J. D. March-Russell and S. M. West, Phys. Lett. **B676**, 133 (2009), 0812.0559.

[38] S. Chang and L. Goodenough, Phys. Rev. **D84**, 023524 (2011), 1105.3976.

[39] K. R. Dienes, J. Kumar, and B. Thomas, Phys. Rev. **D88**, 103509 (2013), 1306.2959.

[40] D. P. Finkbeiner and N. Weiner, Phys. Rev. **D76**, 083519 (2007), astro-ph/0702587.

[41] J. Kopp, Phys. Rev. **D88**, 076013 (2013), 1304.1184.

[42] I. Cholis, D. Hooper, and T. Linden, Phys. Rev. **D95**, 123007 (2017), 1701.04406.

[43] N. Tomassetti and A. Oliva, Astrophys. J. **844**, L26 (2017), 1707.06915.

[44] T. R. Slatyer, N. Padmanabhan, and D. P. Finkbeiner, Phys. Rev. **D80**, 043526 (2009), 0906.1197.

[45] C. Evoli, M. Valdes, A. Ferrara, and N. Yoshida, Mon. Not. Roy. Astron. Soc. **422**, 420 (2012).

[46] M. S. Madhavacheril, N. Sehgal, and T. R. Slatyer, Phys. Rev. **D89**, 103508 (2014), 1310.3815.

[47] P. A. R. Ade et al. (Planck), Astron. Astrophys. **594**, A13 (2016), 1502.01589.

[48] T. R. Slatyer, Phys. Rev. **D93**, 023527 (2016), 1506.03811.

[49] V. Poulin, P. D. Serpico, and J. Lesgourgues, JCAP **1608**, 036 (2016), 1606.02073.

[50] M. Tavakoli, I. Cholis, C. Evoli, and P. Ullio, JCAP **1401**, 017 (2014), 1308.4135.

[51] A. Geringer-Sameth, S. M. Koushiappas, and M. G. Walker, Phys. Rev. **D91**, 083535 (2015), 1410.2242.

[52] M. Ackermann et al. (Fermi-LAT), Phys. Rev. Lett. **115**, 231301 (2015), 1503.02641.

[53] A. U. Abeysekara et al., Astrophys. J. **843**, 40 (2017), 1702.02992.

[54] A. U. Abeysekara et al. (HAWC), Science **358**, 911 (2017), 1711.06223.

[55] A. A. Abdo et al., Astrophys. J. **700**, L127 (2009), [Erratum: Astrophys. J.703,L185(2009)], 0904.1018.

[56] D. Hooper, I. Cholis, T. Linden, and K. Fang, JCAP (2017), [Phys. Rev.D96,103013(2017)], 1702.08436.

[57] T. Linden, K. Auchettl, J. Bramante, I. Cholis, K. Fang, D. Hooper, T. Karwal, and S. W. Li, Submitted to: Phys. Rev. D (2017), 1703.09704.

[58] A. Abramowski et al. (H.E.S.S.), Nature **531**, 476 (2016), 1603.07730.

[59] D. Hooper, I. Cholis, and T. Linden (2017), 1705.09293.

[60] P. M. Dragicevich, D. G. Blair, and R. R. Burman, Mon. Not. R. Astron. Soc. **302**, 693 (1999).

[61] N. Vranesevic et al., Astrophys. J. **617**, L139 (2004), astro-ph/0310201.

[62] C.-A. Faucher-Giguere and V. M. Kaspi, Astrophys. J. **643**, 332 (2006), astro-ph/0512585.

[63] D. R. Lorimer et al., Mon. Not. Roy. Astron. Soc. **372**, 777 (2006), astro-ph/0607640.

[64] E. F. Keane and M. Kramer, Mon. Not. Roy. Astron. Soc. **391**, 2009 (2008), 0810.1512.

[65] I. Cholis and N. Weiner (2009), 0911.4954.

[66] I. Cholis, L. Goodenough, and N. Weiner, Phys. Rev. **D79**, 123505 (2009), 0802.2922.

[67] L. Accardo et al. (AMS), Phys. Rev. Lett. **113**, 121101 (2014).

[68] D. R. Lorimer (2003), [IAU Symp.218,105(2004)], astro-ph/0308501.

[69] R. N. Manchester et al., Mon. Not. Roy. Astron. Soc. **328**, 17 (2001), astro-ph/0106522.

[70] R. N. Manchester, G. B. Hobbs, A. Teoh, and M. Hobbs, Astron. J. **129**, 1993 (2005), astro-ph/0412641.

[71] http://www.atnf.csiro.au/research/pulsar/psrcat.

[72] I. Cholis, D. Hooper, and T. Linden, Phys. Rev. **D93**, 043016 (2016), 1511.01507.

[73] L. J. Gleeson and W. I. Axford, Astrophys. J. **154**, 1011 (1968).

[74] http://www.srl.caltech.edu/ACE/ASC/.

[75] http://wso.stanford.edu/Tilts.html.

[76] R. Trotta, G. Johannesson, I. V. Moskalenko, T. A. Porter, R. R. de Austri, and A. W. Strong, Astrophys. J. **729**, 106 (2011), 1011.0037.

[77] I. Cholis, T. Karwal, and M. Kamionkowski (2018).

[78] L. Bergstrom, T. Bringmann, I. Cholis, D. Hooper, and C. Weniger, Phys.Rev.Lett. **111**, 171101 (2013), 1306.3983.

[79] A. Ibarra, A. S. Lamperstorfer, and J. Silk, Phys. Rev.

[80] J. Chang et al. (DAMPE), Astropart. Phys. **95**, 6 (2017), 1706.08453.

[81] G. Ambrosi et al. (DAMPE) (2017), 1711.10981.

[82] O. Adriani, Y. Akaike, K. Asano, Y. Asaoka, M. G. Bagliesi, G. Bigongiari, W. R. Binns, S. Bonechi, M. Bongi, J. H. Buckley, et al., in *Journal of Physics Conference Series* (2015), vol. 632 of *Journal of Physics Conference Series*, p. 012023.

Appendix A: The Neutron Star Distribution in Space and Time

Ref. [63] suggests that pulsars are born in the Milky Way at a rate of 1.4 ± 0.2 pulsars per century [63], although one finds a wider range of estimates in other work [60–62, 64]. For simplicity we assume a pulsar birth rate of one per century.

The spatial distribution of pulsars in the Galaxy has been investigated in Ref. [62, 63, 68] relying on data from the Parkes multi-beam pulsar survey at 1.4 GHz [69]. Our radial distribution of pulsars is based on the best-fit parameters of Ref. [63], given by an empirical expression for the pulsar surface (column) density in the Galaxy,

$$\rho(R) = A(R/R_\odot)^B \exp\left(-C\frac{R - R_\odot}{R_\odot}\right) \ \text{kpc}^{-2}, \quad \text{(A1)}$$

where R is the Galactocentric radius and $R_\odot = 8.5$ kpc is the distance of the Sun from Galactic center (GC). We use the values $B = 1.9$ and $C = 5.0$ given therein, normalizing A such that we obtain our assumed birth rate. Our spatial simulations are consistent with Ref. [68] as shown in Fig. 4.

Using Eq. (A1), we are lead to the following probability distribution function for the radial distance of a pulsar from GC,

$$PDF(R, B, C) = \frac{C^{B+2}}{Ae^C R_\odot^2} \frac{\rho(R)R}{\Gamma(B + 2)}, \quad \text{(A2)}$$

where $\Gamma(x)$ is a Gamma function. We utilize a Laplace z-distribution with a characteristic scale of 50 pc as done in Ref. [62] and a flat angular distribution and simulate the pulsars within 4 kpc of the Sun.

Appendix B: The Neutron Stars Spin-Down Distribution Properties

Pulsar spin-down powers $\dot{E}$ are calculated using their ages and Eq. 1. The spin-down timescale τ_0 and the braking index κ are varied per set of simulations. We let $\dot{E}_0 = 10^x$ ergs/s with $x = x_{\text{cutoff}} - y$ and where y is taken from a log-normal distribution. The log-normal distribution is generated using the parameters y_μ and y_σ, which are the mean and standard deviation of the underlying Gaussian distribution. We consider four different values
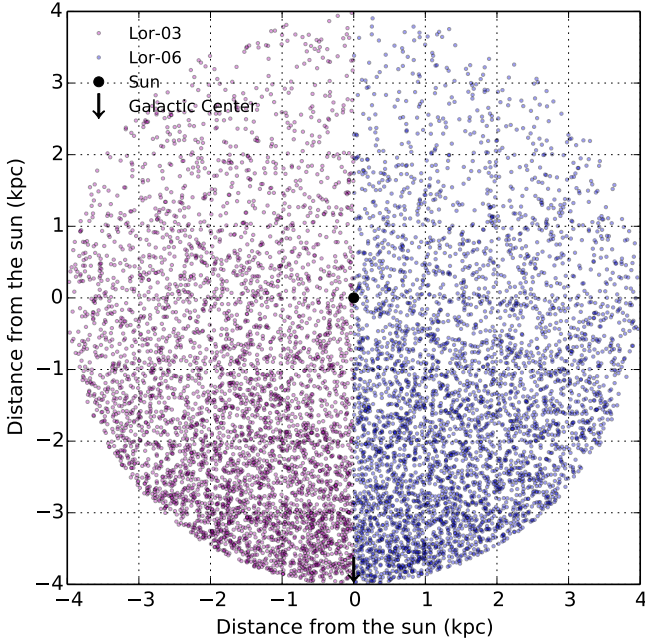
FIG. 4. The pulsars simulated within 4 kpc of the Sun, projected onto the Galactic disk. The Galactic center is at $(0, -8.5)$ kpc. The Sun is the black dot at $(0,0)$. The magenta dots were simulated using the empirical pulsar radial distribution curve presented in Ref. [68]. The blue dots were simulated using the best-fit pulsar radial distribution curve given in Ref. [63]. Both produce very similar results. The number of pulsars in both simulations were normalized such that one per century is born in the Galaxy, showing pulsars up to 10 Myr in age.

Sim no.	τ_0 (kyr)	κ	x_{cutoff}	y_μ	y_σ
30–59	3.3	3	38.8	0.25	0.5
120–149	6	3	38.8	0.25	0.5
150–179	3.3	3	38.8	0.25	0.5
180–209	10	3	38.8	0.25	0.5
210–239	3.3	3	39	0.1	0.5
240–269	1	2.5	38.8	0.25	0.5
270–299	20	3.5	39	0.1	0.5
300–329	0.7	2.5	38.8	0.25	0.5
330–359	20	3.5	39.1	0.0	0.25
360–389	0.6	2.5	39.0	0.1	0.25
390–419	6	3.0	39.0	0.1	0.25
420–449	6	3	38.7	0.5	0.75
450–479	30	3.5	38.8	0.25	0.5
480–509	0.85	2.5	38.5	0.6	0.75
510–539	18	3.5	39.0	0.0	0.75
540–569	10	3	38.7	0.5	0.75
570–599	4	3.0	39.0	0.0	0.36
600–629	1	2.5	38.7	0.5	0.75
630–659	9	3.0	38.2	0.4	0.36
660–689	0.8	2.5	38.2	0.4	0.36
690–719	0.6	2.5	38.2	0.4	0.36
720–749	30	3.5	38.2	0.4	0.36
750–779	7	3.0	39.0	0.1	0.75
780–809	30	3.5	38.0	0.5	0.36
810–839	30	3.5	38.7	0.5	0.75
840–869	6	3	38.9	0.18	0.36
870–899	4.5	3.0	39.3	0.0	0.25
900–929	9	3.0	38.5	0.5	0.25
930–959	27	3.5	38.5	0.3	0.25
960–989	33	3.5	38.0	0.5	0.25
990–1019	0.85	2.5	38.3	0.5	0.25

TABLE II. The assumed pulsar-simulation spin-down power distributions and time evolution. Simulations $\#30 - 59$ are produced based on Ref. [68], while all others are on reference assumption of Ref. [63].

of $y_\sigma = [0.25, 0.36, 0.5, 0.75]$. Values of x_{cutoff} and y_μ are then chosen such that the distributions of observed pulse periods and surface magnetic fields of simulated pulsars are consistent with results presented in Fig. 6 of Ref. [62].

Finally, to ensure that we do not produce pulsars more luminous than the ones recorded in the ATNF catalog [70, 71], we only consider values of $x < x_{\text{max}} = 38.7$. In Table II we give all the spin-down power distribution properties for our pulsar simulations.

Appendix C: The Acceleration of CR electrons and positrons from Pulsars and Injection into the ISM

Electrons get accelerated inside the magnetosphere, produce ICS γ-rays, which in turn in the presence of strong magnetic fields pair produce $e^\pm$. These $e^\pm$ get further accelerated inside the magnetosphere. In addition, electrons and positrons will then propagate outwards losing energy during adiabatic E-losses, but can also be accelerated in the termination shock of the pulsar(also of the SNR) and the ISM. There is also evidence for γ-rays towards Geminga and Monogem [53–55], suggesting the presence of CR $e^\pm$ at 100 TeV in energy, losing a signif-

icant fraction of their energy within $\simeq 10$pc. Since the spin-down power drops with a time-scale of $\tau_0 \lesssim 10^4$ yrs, about half of the rotational energy will be lost before the SNR shock front stops being an efficient accelerator and well before the PWN stops having an effect on these CRs. Given that the time for CR $e^\pm$ to propagate to Earth is an order of magnitude larger than τ_0 we can consider their injection to the ISM instantaneous (see Ref. [20] for further details).

In this work we are agnostic about the fraction η of the spin-down power that goes into injected $e^\pm$. We assume a log-normal distribution for the η parameter,

$$g(\eta) = \frac{Exp\left\{-\frac{[-\mu+ln(-1+\eta)]^2}{2\sigma^2}\right\}}{\sqrt{2\pi}(\eta-1)\sigma}, \qquad (C1)$$

and take three different choices for μ and σ. These lead to three different choices for the combination of mean efficiency η, $\bar{\eta} = 1 + Exp\left\{\mu + \frac{\sigma^2}{2}\right\}$ and logarithmic standard deviation $\zeta = 10^\sigma$: $(\bar{\eta}, \zeta) = (4 \times 10^{-3}, 1.47)$ or $(10^{-3}, 2.85)$ or $(2 \times 10^{-2}, 1.29)$. As described in the main text, in fitting the positron fraction we allow for

Model	b ($\times 10^{-6}$ GeV^{-1}kyrs^{-1})	D_0 (pc^2/kyr)	δ
A1	5.05	123.4	0.33
C1	5.05	92.1	0.40
C2	8.02	92.1	0.40
C3	2.97	92.1	0.40
E1	5.05	58.9	0.50

TABLE III. The basic parameters that describe the propagations assumptions of cosmic rays in the Milky Way. Assuming isotropic and homogeneous diffusion, $D(R) = D_0(R/1GV)^\delta$. The energy losses due to synchrotron radiation and inverse Compton scattering are described by $dE/dt = -b\,E^2$.

each astrophysical pulsar realization an overall normalization change in the pulsar component, that is absorbed into the specific values of $\bar{\eta}$. Our typical $\bar{\eta}$ is a few$\times 10^{-2}$ with a range of $2 \times 10^{-3} - 2 \times 10^{-1}$.

For the injection CR $e^\pm$ spectra we assume,

$$\frac{dN}{dE} \propto E^{-n} Exp\left\{ -\frac{E}{E_{\text{cut}}} \right\}, \qquad \text{(C2)}$$

with n following a flat distribution $g(n)$ either in a narrow range of $n\epsilon\,[1.6, 1.7]$ or in a wider range of $n\epsilon\,[1.4, 1.9]$. The upper cutoff E_{cut} does not affect our fits to the observations, since the highest-energy CR $e^\pm$ quickly lose their energy before reaching us; we set it to $E_{\text{cut}} = 10$ TeV.

Appendix D: Cosmic-Ray Propagation through the ISM and heliosphere

From the moment CRs enter into the ISM they diffuse through the Milky Way magnetic field and suffer energy losses due to synchrotron radiation and inverse Compton scattering. We use five distinctive models for the ISM that agree with CR data including the B/C ratio, CR protons and He [72]. The characteristics of these five ISM models are given in Table III.

The impact of these uncertainties on the morphology of the CR spectra is shown in Figure 5 for the positron fraction (colored lines). Depending on the assumptions on the energy losses and diffusion time-scales, the spectral features can be more pronounced or suppressed.

Once exiting the ISM and entering the heliosphere, CRs will reach our detectors, after diffusing through the anisotropic magnetic-field structure of the fast evolving heliospheric magnetic field. During their propagation through the heliosphere, CRs also transfer via drift effects that impact how fast they will reach Earth, and the path they are most prone to follow through the Heliosphere. During that time CRs will also go through adiabatic energy losses. The effect of solar modulation on

CR spectra is described by the solar-modulation potential Φ that describes the average energy losses CR suffer as they travel through the Heliosphere. That, in terms
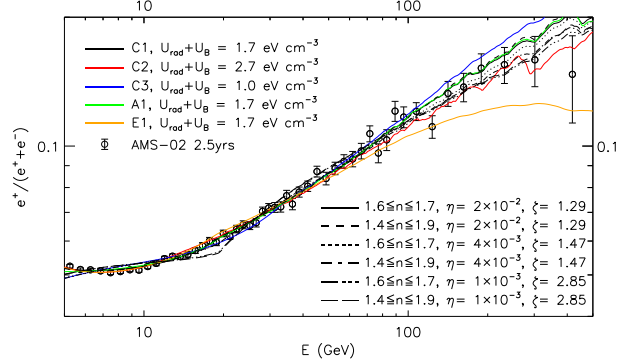

FIG. 5. The positron fraction, assuming pulsars follow the same distribution in space and in their spin-down power and time evolution. We vary the ISM propagation conditions (different colors) as in Table III, and the CR $e^\pm$ spectral properties and fraction of spin-down power into ISM injected $e^\pm$. $U_{\text{rad}} + U_{\text{B}}$ refer to the local energy density in the radiation and magnetic fields. Some of these lines are excluded in the positron fraction spectrum fit and are not used further in the PSD analysis.

of CR spectra, is given by [73],

$$\frac{dN^\oplus}{dE_{kin}}(E_{kin}) = \frac{(E_{kin} + m)^2 - m^2}{(E_{kin} + m+ \mid Z \mid e\Phi)^2 - m^2}$$
$$\times \frac{dN^{\text{ISM}}}{dE_{kin}}(E_{kin}+ \mid Z \mid e\Phi). \qquad \text{(D1)}$$

Here, E_{kin} is the kinetic energy at Earth, and $\frac{dN^{\oplus(\text{ISM})}}{dE_{kin}}$ are the differential CR fluxes observed at Earth ($\oplus$) and the local interstellar medium (ISM) respectively. Finally, $\mid Z \mid e$ is the absolute charge of CRs.

Ref. [72], using proton fluxes from 1992 and up to 2010, resulted in the predictive, time-, charge- and rigidity(R)-dependent formula for the solar modulation potential,

$$\Phi(R, q, t) = \phi_0 \left(\frac{\mid B_{\text{tot}}(t) \mid}{4\,\text{nT}} \right) + \phi_1\, H(-qA(t)) \left(\frac{\mid B_{\text{tot}}(t) \mid}{4\,\text{nT}} \right)$$
$$\times \left(\frac{1 + (R/R_0)^2}{\beta (R/R_0)^3} \right) \left(\frac{\alpha(t)}{\pi/2} \right)^4, \qquad \text{(D2)}$$

with R_0 set to 0.5 GV and with a 2σ range for ϕ_0 of 0.32–0.38 GV and ϕ_1 in the range of 0–16 GV. We marginalize over these ranges of ϕ_0 and ϕ_1. In Eq. D2 we use the values of $B_{\text{tot}}(t)$ and $\alpha(t)$ measured by ACE [74] and modeled in WSO [75]. Having these values, we can directly calculate the $\Phi(R, q, t)$, for any CR species at a given rigidity and time t. For further details see [72].